Sensors and Actuators: A. Physical 332 (2021) 113047

Contents lists available at ScienceDirect

Sensors and Actuators: A. Physical

journal homepage: www.elsevier.com/locate/sna

Design and development of a microfluidic droplet generator with vision sensing for lab-on-a-chip devices

Samith Hettiarachchi[a,*], Gehan Melroy[a], Amith Mudugamuwa[a], Peshan Sampath[a], Charith Premachandra[b], Ranjith Amarasinghe[a,b], Van Dau[c]

[a] Centre for Advanced Mechatronic Systems, University of Moratuwa, Katubedda 10400, Sri Lanka
[b] Department of Mechanical Engineering, University of Moratuwa, Katubedda 10400, Sri Lanka
[c] School of Engineering and Built Environment, Griffith University, Australia

ARTICLE INFO

Article history:
Received 19 April 2021
Received in revised form 25 June 2021
Accepted 16 August 2021
Available online 26 August 2021

Keywords:
Active droplet generator
Microfluidics
Lab-on-a-chip
Flow-focusing
Vision sensing

ABSTRACT

Lab on a Chip (LOC) devices minimize, integrate, automate, and parallelize laboratory functions such as mixing, separation, and incubation on a single chip. Droplet generation is one key aspect in LOC devices which allows to conduct various chemical and biochemical assays enabling biological cell studies, high throughput drug development, and diagnostic screenings. This paper presents, modelling, simulation, and experimentation of an active droplet generator that is widely used in LOC devices. The model geometry used in this study was based on a flow focusing method of droplet generation. Droplet generation from the numerical simulations was observed within flow rate ratios ranging from 0.2 to 4 using optimised droplet contraction width of the generator model. Subsequently, a prototype droplet generator was designed and developed from Polymethyl Methacrylate (PMMA) material using a layer-based fabrication method. Based on the experimental setup presented here, the calculated ratios of flow rates obtained for different voltage values have shown that the formation of droplets occur between flow rate ratios of 1.04 and 4.74. In addition, morphological parameters of the droplet images extracted from a digital image processing algorithm show that the mean diameter of the droplets decreases with decreasing flow rate ratios.

1. Introduction

The evolution of miniaturized fluidic systems and the development of microfluidic devices over the past decade have been under the attention of the biomedical research community [1]. As an interdisciplinary area, this rapidly growing field of technology has found numerous applications in biomedical engineering including pathology, therapeutics, drug delivery, biosensors, and tissue engineering [2,3]. One of the pivotal applications of microfluidics is the development of Lab-on-a-Chip (LOC) devices as point-of-care diagnostic tools.

A typical LOC device includes various functional modules: sample transportation and preparation module, separation module, and detection and analysis module [4]. The separation modules play important roles in preparative applications where samples are purified through separation of biological objects, and are used in analyses where these separated objects are studied thoroughly. In addition, size-based sorting of objects in a sample is one of the important techniques used in the fields such as industrial, production, food and chemical industry, environmental assessment and chemical or biological research. Therefore, among all microfluidic systems, droplet generation systems have inspired many researchers leading to various innovations [5,6]. The droplet generation systems focus on creating discrete volume with the use of immiscible phases. Since, droplet-based microfluidic systems provide independent controllability of each drop, these systems are used for individual analysis, mixing, and transportation of droplets or fluids [7]. The manipulated droplets having volumes in nanoliter or femtoliter range can act as isolated reaction containers for biochemical assays [8]. In most of the applications, highly uniform droplets are desired to ensure constant, controlled, and predictable outcomes. Therefore, formation of uniform droplets in a controllable manner is the most significant aspect of a microfluidic droplet generation system.

Flow rate ratio, capillary number, viscosity ratio, interfacial tension between the two immiscible fluids, wetting properties of the

* Corresponding author.
E-mail addresses: samithhettiarachchi58@gmail.com (S. Hettiarachchi), nhrgmelroy@gmail.com (G. Melroy), amith.mudugamuwa@gmail.com (A. Mudugamuwa), peshan@ieee.org (P. Sampath), charithpremachandra95@gmail.com (C. Premachandra), ranamajp@gmail.com (R. Amarasinghe), v.dau@griffith.edu.au (V. Dau).

https://doi.org/10.1016/j.sna.2021.113047
0924-4247/

channel walls, and the channel geometry are the most important parameters which influence the droplet generation process [9]. The droplet generation can be divided into two main groups based on the specific energy consumption of the droplet: passive droplet generators use hydrodynamic pressure of the flow without an external power input, and active droplet generators use external power inputs to produce droplets. The active droplet generators are further categorized into electrically, thermally, magnetically, and mechanically operated depending on the working principle. The droplet generators that are mechanically operated, involve physical deformation of the liquid interface using hydraulic, pneumatic, or piezoelectric actuation [10,11]. Additionally, transportation of the fluid is divided into active and passive depending on the actuation or driving force. According to the literature, active transporters have better controllability over the passive transporters [12].

Computational Fluid Dynamics (CFD) is an area of study in fluid mechanics that uses mathematical models and numerical simulations to analyze fluid flow characteristics [13]. Therefore, multiple techniques to analyze the behaviour of two phase fluid flows have been discussed and are applicable in simulating droplet generation. In fabricating microfluidic devices, micromachining, lithography, embossing and imprinting, injection molding, laser-based, and additive manufacturing based methods are widely discussed in literature [14]. Laser-based methods are used to fabricate microfluidic droplet generators because of the simplicity, versatility, and time efficient nature compared to other low volume fabrication methods [15]. Polydimethylsiloxane (PDMS) and PMMA materials are used in fabricating microfluidic channels because of the biocompatibility, transparency, and the comparative low cost [16].

Among various sensing methods, vision sensing is emerging as it has a wide range of applications such as object detection, abnormality identification, feature extraction, and path planning. Remote monitoring, controlling, and analysis are the major advantages achieved using vision sensing [17]. Currently, macro and micro imaging technologies have been the focus areas associated with the application of telemedicine in the literature. Digital image processing includes pre-processing of captured digital images, feature extraction, and results analysis. Therefore, digital image processing is implemented as the sensing method in droplet based microfluidic systems to extract morphological features of the droplets, study the system performance, and to control droplet generation in real-time. Feedback control based droplet generators provide higher degree of controllability for the droplet generation process. In addition, automatic feedback control systems consist of closed loop feedback using PID control provide real-time controllability, higher accuracy, and reliability to the droplet based microfluidic systems [18].

Therefore in this study, an active droplet generator with microfluidic flow-focusing geometry was designed, developed, numerically and experimentally analyzed in order to optimize the contraction channel width and the flow rate ratio in the droplet generation of proposed geometry.

2. Proposed system and the working principle

As shown in Fig. 1, the proposed active microfluidic droplet generation system comprises three (03) stages viz pumping, droplet generation, and vision based sensing and data acquisition.

2.1. Proposed droplet generator

The proposed design of the droplet generator shown in Fig. 2 is capable of injecting two fluids into the microfluidic channel. The inlet - A is for the dispersed phase fluid and the inlet - B is for the continuous phase fluid. The contraction (as detailed in Fig. 2) where the two fluids are touched, acts as the geometrical constraint that generates droplets. Then the generated droplets are channeled through the cavity that terminates at outlet - C, and is used for sensing and data acquisition.

The dominant parameters of the contraction geometry can be identified as contraction channel width (w), contraction channel length (l), and fillet radius (R) as shown in Fig. 2. In the proposed design, length of the contraction channel is 2.5 mm, fillet radius is 0.5 mm, channel depths are 1 mm, all the inlet channel widths are 4 mm, and the outlet channel width is 6 mm.

2.2. Working principle

Cross-flow, co-flow, and flow-focusing are the most widely used geometries that breakoff droplets with the effect of viscous shear forces [19]. In cross-flow geometry, dispersed and continuous phase fluids meet at an angle. This is frequently implemented as a T-junction where the two fluids meet at 90-degree angle. In co-flow geometry, both fluid streams are parallel before mixing. In the flow-focusing geometry, two fluids are hydrodynamically focused into a contraction. Droplets are formed due to the elongating flows when passing through a contraction. The flow-focusing devices are capable of generating smaller droplets in a more controllable and stable manner compared to aforementioned geometries.

In flow-focusing geometry, the continuous phase fluid distracts the dispersed phase fluid at the entrance of the contraction. When the applied shear stresses are greater than that of the viscosity, the dispersed phase flow breaks into droplets. This process is divided into four main steps such as lagging, filling, necking, and detachment. In the lagging step, the dispersed phase is in its inlet where it has not reached the contraction. The filling stage is where the dispersed phase penetrates into the contraction. In the necking stage the continuous phase fluid applies shear stress on the dispersed phase while it elongates in the contraction. Detachment is where the droplets break up, when the applied shear stress is greater than the viscosity. The flow-focusing geometry and the contraction used in the proposed design are highlighted in Fig. 2.

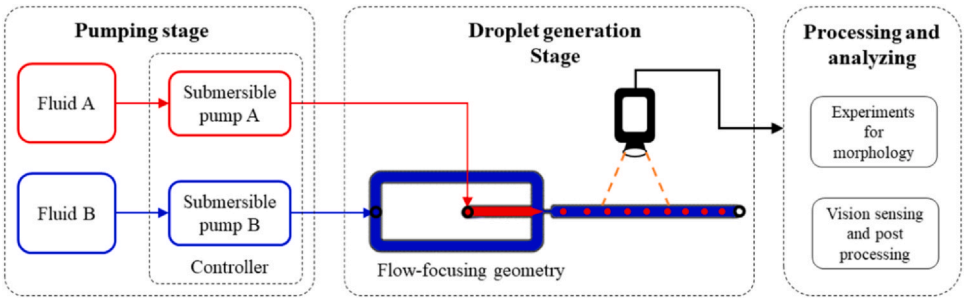

Fig. 1. Proposed overview of the system.

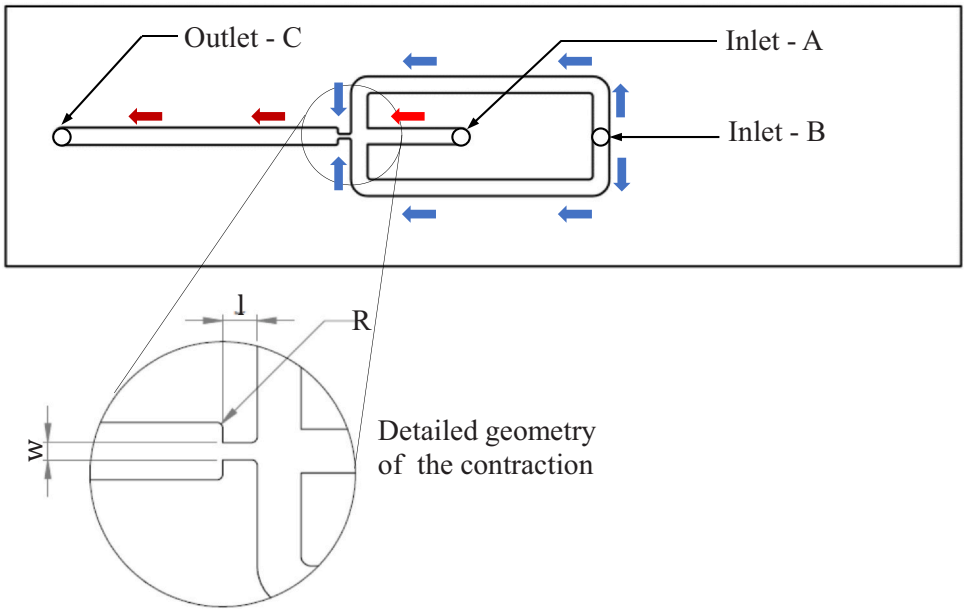

Fig. 2. Droplet generation geometry.

3. Modelling and simulation

The level set technique presents the significant advantage of having a smoothing function in identifying the regions of the two phases resulting a minimum error in determining the location of the interface which is critical to calculate the surface tension force. Therefore, the level set technique is used in simulating droplet generation using microfluidic flow focusing geometries. Simulations were conducted by varying the width of contraction channel in the flow-focusing geometry (shown in Fig. 2) which was designed in the former stage of the research [20] to obtain the optimum contraction width. The level set method in COMSOL Multiphysics was used for the analysis.

3.1. Numerical modelling

In this study, the conservative level set method was used to simulate the droplet generation of the proposed microfluidic flow-focusing geometry. The conservative level set method addresses the drawback of conventional level set method being non-conservative [21]. The level set equation Eq (1) is:

$$\frac{\partial \phi}{\partial t} + \vec{u}\cdot\nabla\phi = \gamma\nabla\cdot\left[\varepsilon\nabla\phi - \phi(1-\phi)\frac{\nabla\phi}{|\nabla\phi|}\right], \tag{1}$$

where, the level-set function ϕ is in the range of 0–1. $\phi = 0$ indicates the phase 1 fluid and $\phi = 1$ indicates phase 2 fluid. ϵ is the thickness of the interface, and it varies with the phase change. Iteration number of the level set function reinitialization is given by γ and the velocity of the phase field is given by $\vec{u}$.

As both fluids used in this study were assumed to be incompressible and Newtonion, Navier-Stokes equation Eq (2) was used as the governing equation to describe the flow behaviour. The Navier-Stokes equation establishes the equilibrium between momentum and shear forces acting on a control volume. Furthermore, density and the dynamic viscosity of water and coconut oil were assumed to be constant in the analysis. Continuity equation Eq (3) was also used to describe the flow as the total inflow of liquids is equal to the total outflow.

$$\rho\frac{\partial \vec{u}}{\partial t} + \rho(\vec{u}\cdot\nabla)\vec{u} = -\nabla P + \mu\nabla^2\vec{u} + \vec{f} \tag{2}$$

$$\nabla\vec{u} = 0 \tag{3}$$

P, μ, and ρ denotes pressure, dynamic viscosity, and the density of the fluid. Left hand side of the Eq (2) describes the rate of change of momentum and right-hand side ∇P term represents the pressure force, $\mu\nabla^2\vec{u}$ term expresses the viscous force and the term $\vec{f}$ for other body forces acting on the particles such as gravitational force and surface tension force.

The surface tension force acting on the interface between the fluids is calculated as shown in Eq (4).

$$\vec{F} = \sigma\kappa\delta\hat{n} \tag{4}$$

Interfacial tension coefficient is σ and κ is the curvature which is calculated as in Eq (5) where, δ is the Dirac delta function which is acquired by a smooth function determined as in Eq (6). $\hat{n}$ is the unit normal vector to the interface Eq (7).

$$\kappa = -\nabla\cdot\hat{n}|_{\phi=0.5} \tag{5}$$

$$\delta = 6|\nabla\phi||\phi(1-\phi)| \tag{6}$$

$$\hat{n} = \frac{\nabla\phi}{|\nabla\phi|} \tag{7}$$

The density and viscosity of the flow varies smoothly over the interface, which are described in Eqs. (8) and (9).

$$\rho = \rho_1 + (\rho_2 - \rho_1)\phi \tag{8}$$

$$\mu = \mu_1 + (\mu_2 - \mu_1)\phi \tag{9}$$

ρ_1 and ρ_2 are the density of phase 1 and phase 2 whereas, μ_1 and μ_2 are the dynamic viscosity of phase 1 and phase 2, respectively.

3.2. Numerical simulations

COMSOL Multiphysics 5.5 software was used for numerical simulation of the microfluidic flow focusing geometry of the proposed droplet generator geometry in section 2. In general, laminar flow behaviour is observed due to the characteristic length scale of microfluidic devices. Therefore, the simulation was conducted in a two-dimensional domain in laminar two-phase level set method under CFD module in COMSOL Multiphysics. As two immiscible fluids are required for droplet generation, water and coconut oil were selected

Table 1
Physical properties of the selected liquids.

Description	Liquid	Density (kg/m^3)	Dynamic Viscosity (cP)
Dispersed phase	Water	1000	1.01
Continuous phase	Coconut oil	900	55

as dispersed phase and the continuous phase fluids respectively. The physical properties of the selected fluids are show in Table 1. The selected fluids were considered as incompressible, Newtonian and the walls were defined as wetted walls in the simulation. The simulation was conducted with both phase initialisation and time dependent studies providing constant flow velocities for two fluid inlets and setting the outlet pressure to zero.

At first, numerical simulations were conducted to observe the effect of expansion ratio for droplet generation in a flow-focusing geometry. Expansion ratio is defined as the ratio between contraction width and downstream (outlet channel) width. The analysis was carried out for 1.0 mm, 1.5 mm, 2.0 mm, and 2.5 mm contraction channel widths, having the downstream width as a constant. Droplet generation pattern was observed for a fixed flow rate for all geometries. The Fig. 3 shows simulation results for the four different contraction widths considered in this research. A significant variation was observed in droplet generation for different contraction widths. The geometry with the contraction width of 2.0 mm that has an expansion ratio of 1/3 was able to perform the droplet breakup preferably compared to other discussed geometries. From the simulations conducted for the selected contraction widths, the geometry that has a 2.0 mm contraction width showed the minimum time to breakup droplets. Therefore, it was identified that the geometry which has a contraction channel width of 2 mm is suitable for the design.

After finalising the contraction width of the geometry, numerical simulations were conducted to identify the suitable ratios for the flow rates in order to generate droplets. Flow rate ratio was defined as the ratio between the flow rate of the dispersed phase fluid (Q_D) and the flow rate of the continuous phase fluid (Q_C). The results were used to identify the range of flow rate ratios (Q_D/Q_C) for droplet generation. According to the simulation results, flow rate ratio ranges from 0.2 to 4.0 is suitable for droplet generation in the selected flow-focusing geometry. Omid et al. [22] conducted a similar numerical analysis to study the effect of channel geometry and fluid velocity on droplet generation in flow-focusing geometries. The Fig. 4 shows the simulation results obtained for different flow rate ratios.

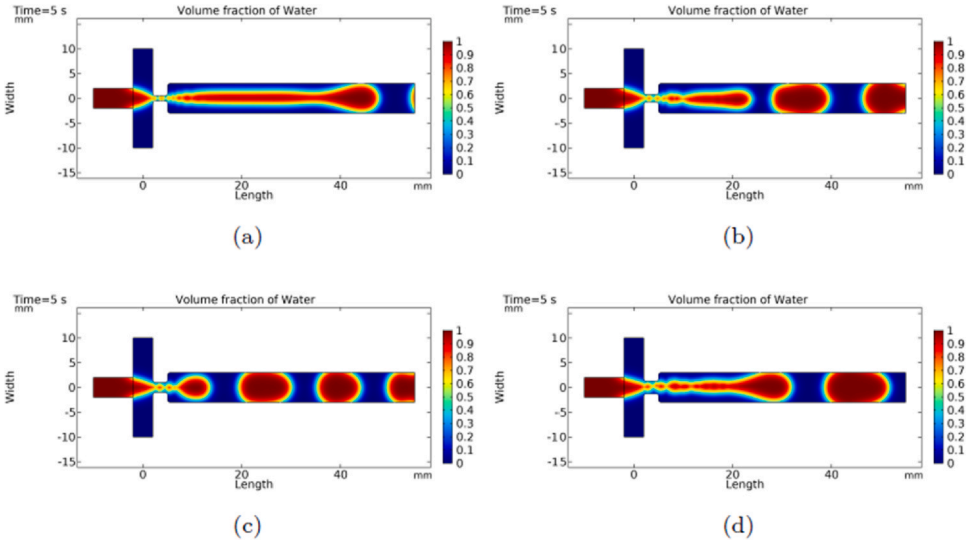

Fig. 3. Droplet breakup for different contraction widths: (a) 1.0 mm; (b) 1.5 mm; (c) 2.0 mm; (d) 2.5 mm.

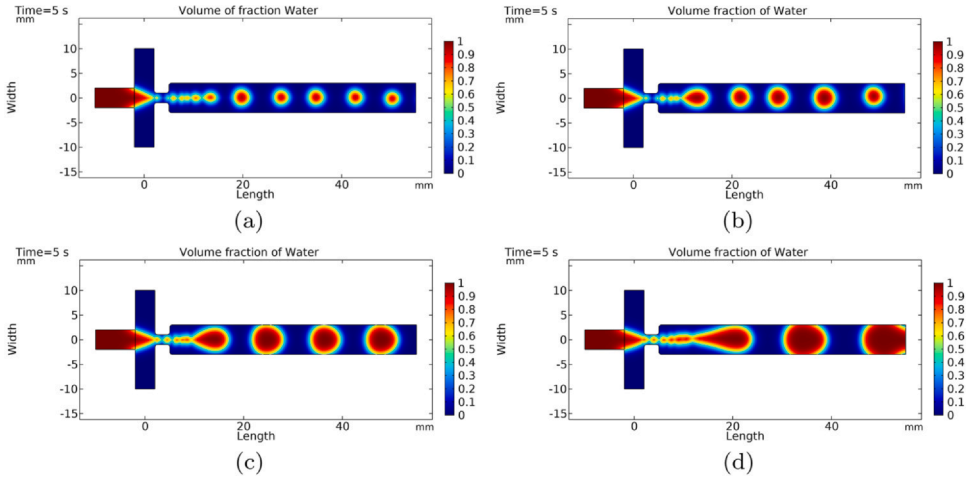

Fig. 4. Simulation results of generated droplet for different flow rate ratios: (a) $Q_D/Q_C = 0.5$; (b) $Q_D/Q_C = 1$; (c) $Q_D/Q_C = 2$; (d) $Q_D/Q_C = 4$.

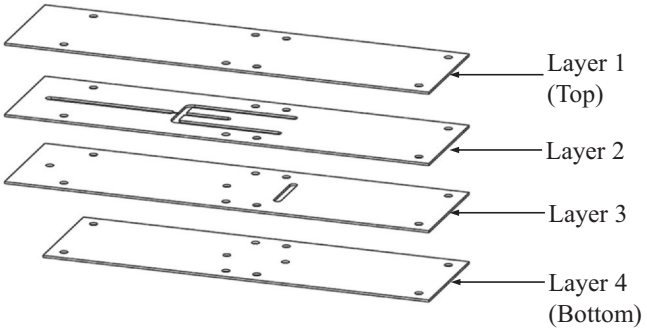

Fig. 5. Exploded view of the droplet generation assembly.

4. Fabrication and assembly

4.1. Fabrication of the droplet generator

The droplet generator design was split into four (04) layers (shown in Fig. 5), layer 1 (top) and layer 4 (bottom) act as sealings for fluid flowing channels, whereas layer 2 and 3 together produce the channel geometry.

Four layers were proposed to increase fabrication simplicity than using complex mask fabrication methods. PMMA was used as the fabrication material because it has the advantages of biocompatibility, easy to clean, and is reusable in multiple instances. Laser cutting technology was used to fabricate individual layers using PMMA sheets with 1 mm thickness because of the advantages such

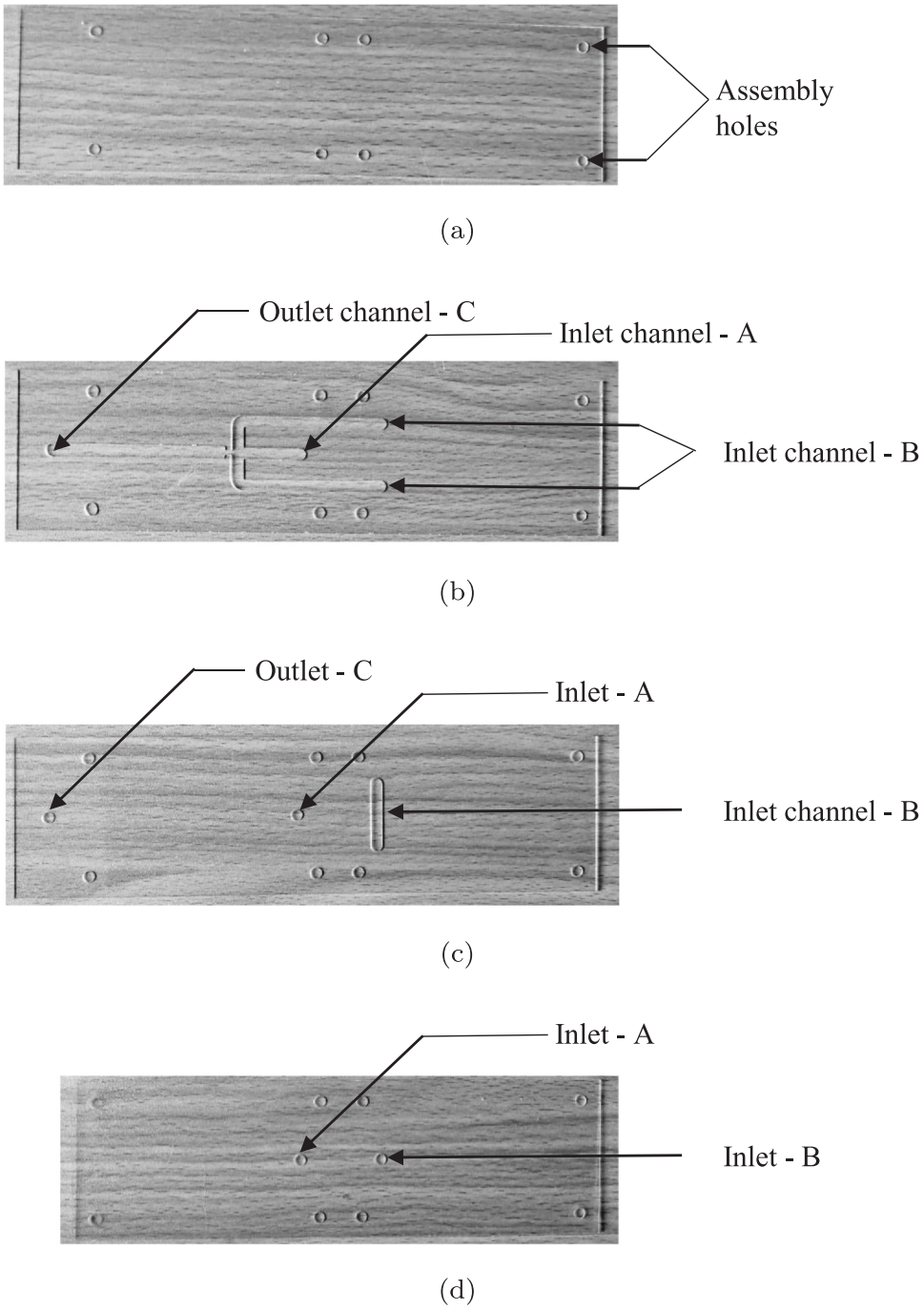

Fig. 6. PMMA layers fabricated using laser cutting technology: (a) Layer 1; (b) Layer 2; (c) Layer 3; (d) Layer 4.

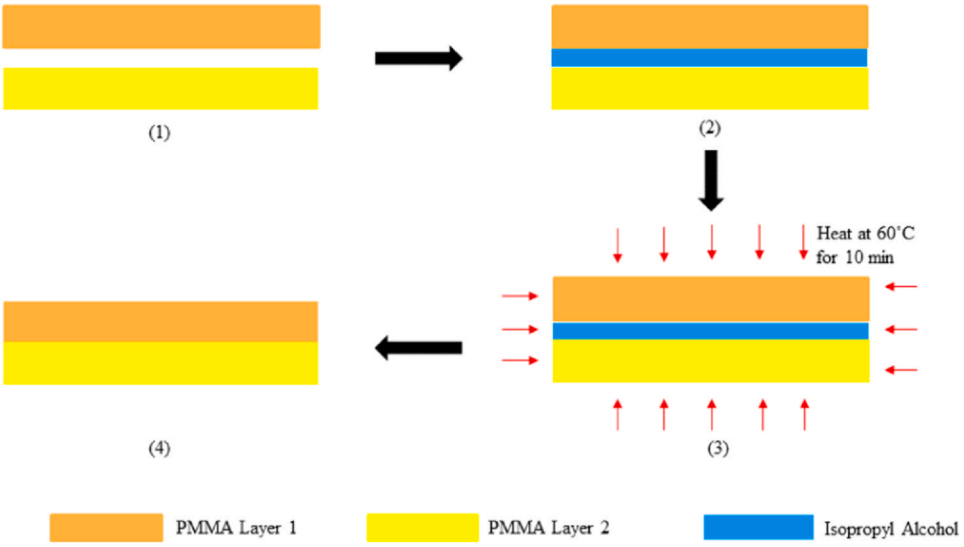

Fig. 7. Bonding process of two PMMA layers.

as less time consumption and cost effectiveness compared to other fabrication techniques. The fabricated PMMA sheets after laser cutting are shown in Fig. 6.

In order to bond the PMMA layers together a simple and solvent assisted method was used [23]. At first, isopropyl alcohol was used to remove dust and other particles deposited on the surface of all PMMA layers and also isopropyl alcohol was used as the binding medium. After applying isopropyl alcohol on the binding surfaces, PMMA layers were clamped together and heat-treated. The treatment was conducted at a temperature of 60°C for ten minutes for proper bonding without any leakages, deformation or air bubbles between the layers [24]. The Fig. 7 shows the steps followed in fabrication.

4.2. Assembly of the active droplet generation system

Active droplet generation requires an external energy for actuation. Therefore, two fluids were pumped to the droplet generator using two submersible type pumps attached to both dispersed phase and continuous phase separately. Operating voltage of the submersible pumps are 2.5–6 V while the rated current is 0.18 A. It generates the fluid flow by converting rotary energy into kinetic energy which is then converted to pressure energy. At first, the fluid is pulled into the pump due to the generated fluid pressure difference and then the rotating impeller pumps the fluid through a diffuser. The flow rate of the submersible pump is varied by changing the supply voltage. Compared to the peristaltic pumps which are widely used in microfluidic applications, submersible pumps present minimum cyclic fluctuations in the flow rate. Submersible pumps have a lower response time and the ability to provide continuous pumping, to increase the controllability with respect to syringe pumps. Additionally, submersible pumps do not require priming which minimise the failure of the pumps due to dry run [25,26]. The schematic diagram of the assembly is shown in Fig. 8

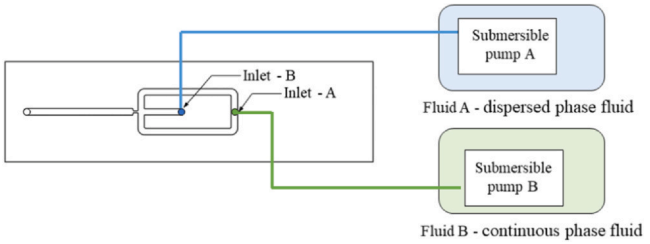

Fig. 8. Schematic diagram of the active droplet generation system.

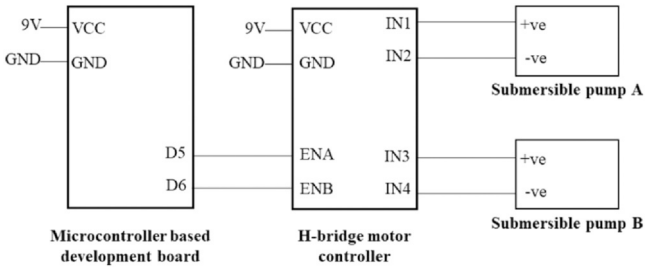

Fig. 9. Circuitry used with the active droplet generation system.

In addition to the two submersible type pumps, a ATmega328P based microcontroller development board, H-bridge motor controller, and a power supply was used to vary flow rates and generate droplets in a controlled manner. The circuitry used with the active droplet generation system is shown in the Fig. 9.

5. Vision based sensing and data acquisition

Image acquisition, pre-processing, and data acquisition are identified as the major steps in morphological feature extraction of droplets. Depending on the droplet sizes, micro or macro imaging methods are used to acquire images of droplets. Camera with a complementary metal oxide semiconductor (CMOS) image sensor was used to capture macro scale images the outlet channel of the droplet generator. Images of the outlet channel were acquired having the camera placed above the droplet generator, therefore images were captured with the plan view. Initially, images captured using the experimental setup were pre-processed in three stages which are cropping, enhancing, and marking. Depending on the original image, several enhancing methods were used as necessary to increase the visibility of droplets. Droplets which were not deformed were marked, and a square was marked in between the channel as the reference geometry because the outlet channel width is a known parameter.

Length of a side of the reference square was used to calculate the dots per millimeter (dpmm) value Eq (10).

$$dpmm = \frac{Length\ \ of\ \ a\ \ side\ \ in\ \ square\ \ (pixels)}{Channel\ \ width\ \ (mm)}, \tag{10}$$

Area and perimeter of each droplet were calculated using the image processing algorithm and then, an average diameter was calculated Eq (11).

$$Diameter\ (d) = \frac{Diameter\quad (Area) + Diameter\quad (perimeter)}{2}, \tag{11}$$

Average diameter values were obtained in pixels, and were converted to millimeter using the dpmm value.

6. Experiments

6.1. Experimental procedure

Initially, experiments were conducted on each fluid to assess the flow rates at different voltage values. This was carried out for the purpose of producing reference graphs to obtain the flow rates under different voltage values. During the experiment, fabricated droplet geometry and pumps heads were maintained at the same level. The experiments were conducted to generate droplets for different flow rate ratios and acquire data related to the generated droplets. During the experiments, morphological properties (i.e. droplet diameter and shape) as well as content and concentration details of the generated droplets were observed. The setup used for experiments is shown in Fig. 10.

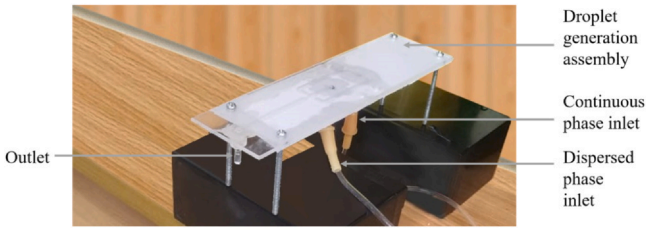

Fig. 10. Experimental setup.

6.2. Calculating droplet diameter based on image processing

Diameters of droplets in each image were calculated based on digital image processing using MATLAB software. Resulting images of a sample image in cropping, enhancing, and marking stages are shown in Fig. 11(a–c), respectively.

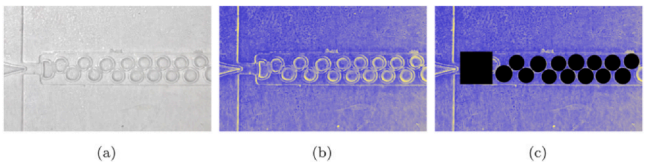

Fig. 11. Image preprocessing: (a) Cropping; (b) Enhancing; (c) Marking.

Reading a marked image, converting to a grayscale image, object identification, and extracting features of the droplets are the main steps in the image processing algorithm developed for calculating the droplet diameter. Aforementioned steps are shown in Fig. 12.

7. Results and discussion

Flow characteristics obtained with reference to different voltage values during separate experiments for two different phases, are shown in Figs. 13 and 14. In obtaining the flow characteristics, water and coconut oil were separately pumped by providing different voltage values to the submersible pumps. The experiments were conducted repeatedly for three times and the flow rates were averaged in determining the flow rate curves. The obtained flow characteristics were used in the droplet generation experiment.

In the experiment, pumping voltage values which generate droplets were identified. Obtained pumping voltage values were used to find flow rate values with reference to the graphs shown in Figs. 13 and 14. According to flow rate values obtained using the graphs, the respective flow rate ratios (Q_D/Q_C) were calculated and shown in Table 2.

Captured images of the generated droplets in the experiment for various flow rate ratios are shown in Fig. 15.

Considering the 6 mm width of the outlet channel, droplet diameters in each image were calculated and the variation of the diameters with respect to different flow rate ratios are shown in Fig. 16.

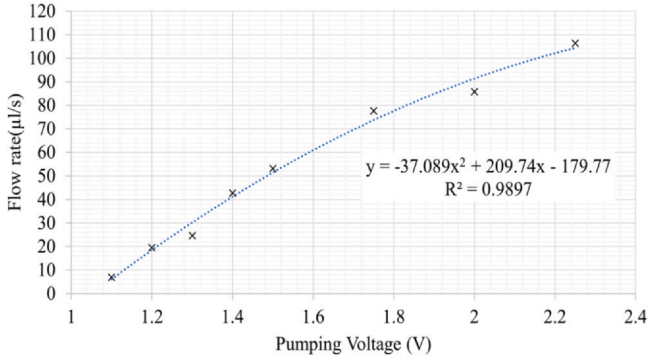

Fig. 13. Flow rate vs pumping voltage for dispersed phase.

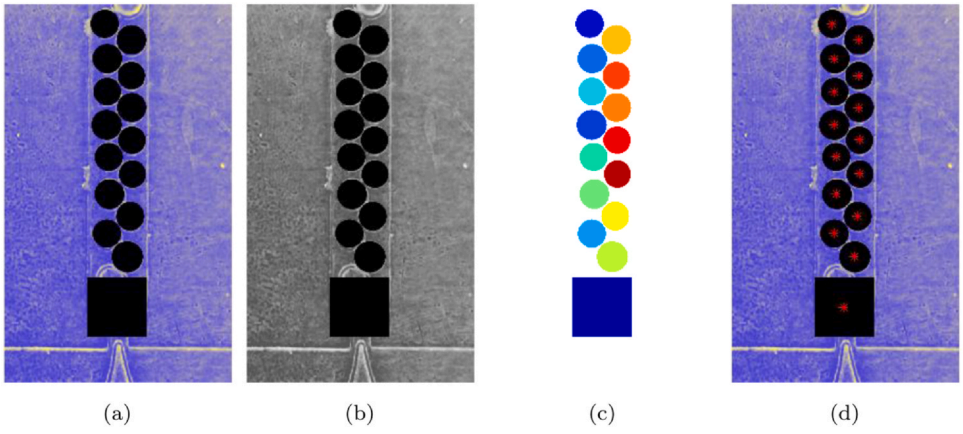

Fig. 12. Processing sequence of droplet detection and feature extraction: (a) Marked image; (b) Grayscale image; (c) Object detection; (d) Feature extraction.

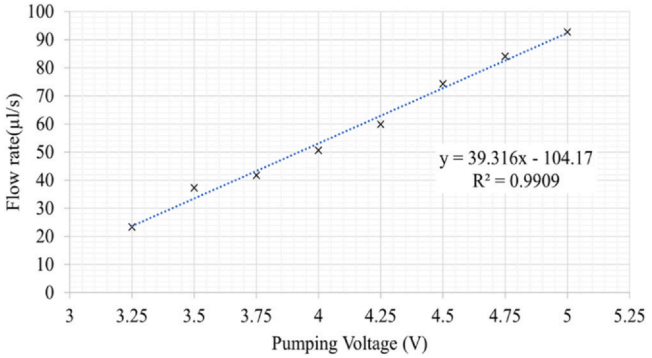

Fig. 14. Flow rate vs pumping voltage for continuous phase.

Table 2
Flow rate ratios against different voltage values.

Voltage (V)		Flow rate ($\mu l/s$)		Flow rate ratios (Q_D/Q_C)
Dispersed phase	Continuous phase	Q_D	Q_C	
1.65	4.25	65	63	1.04
2	4	91	53	1.72
2.05	3.75	94	43	2.18
2	3.5	91	33	2.73
1.9	3.25	85	24	3.59
1.65	3	65	14	4.74

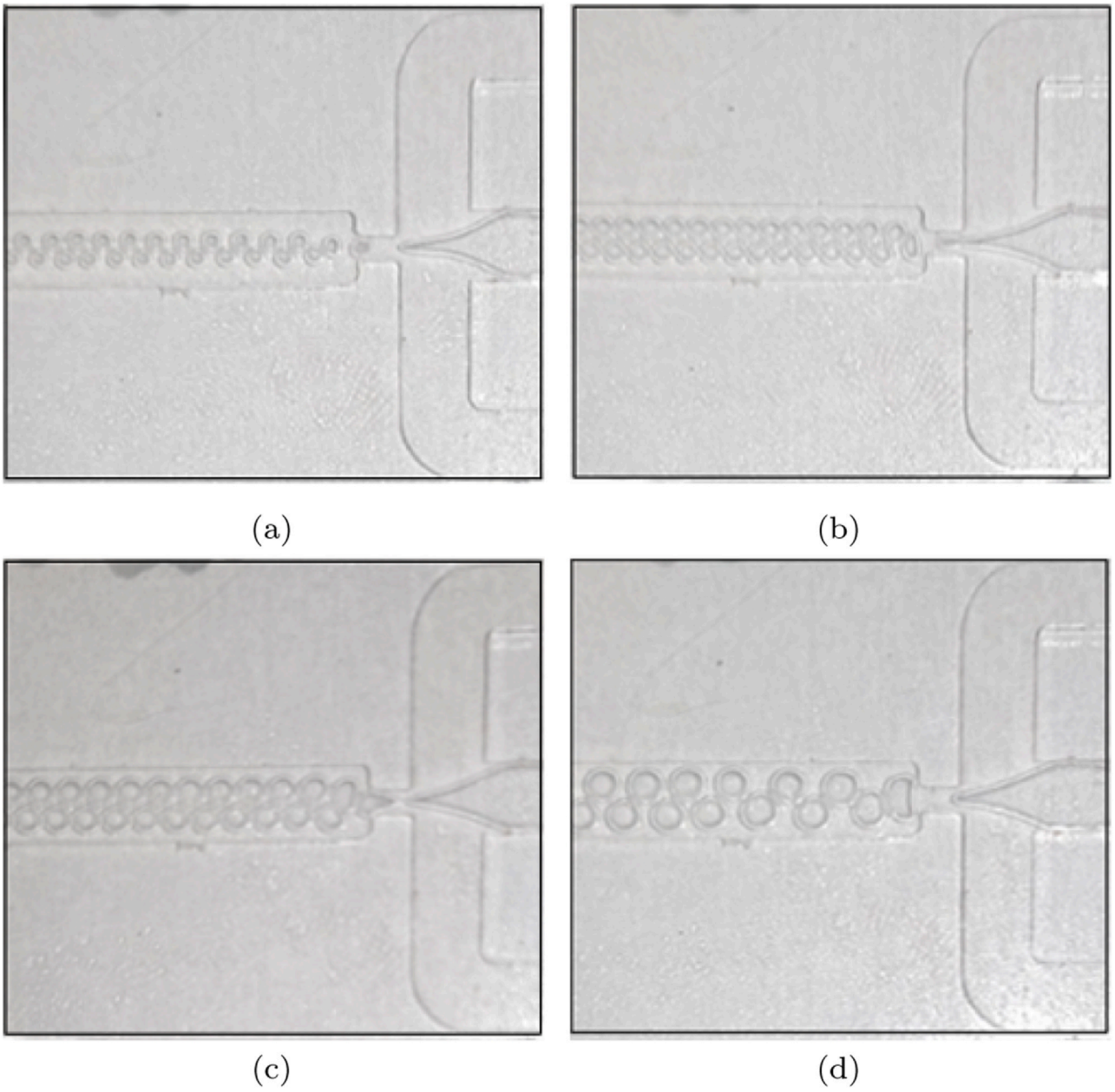

Fig. 15. Observed droplet patterns for different flow rate ratios: (a) $Q_D/Q_C = 1.72$; (b) $Q_D/Q_C = 2.18$; (c) $Q_D/Q_C = 2.73$; (d) $Q_D/Q_C = 4.74$.

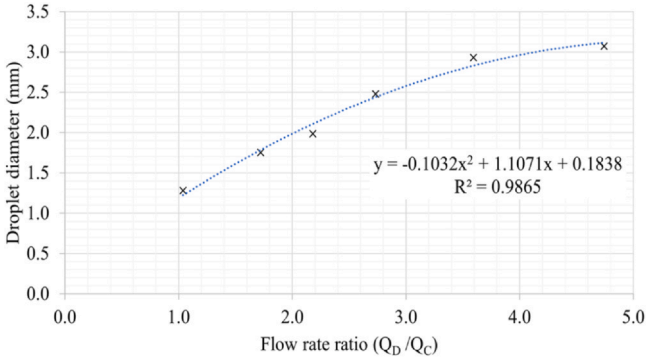

Fig. 16. Flow rate ratios vs droplet diameter.

8. Conclusion

In this study, an active droplet generator was designed, simulated, fabricated, and experimented. Contraction channel width of the geometry was optimised by the numerical simulations and it was concluded that the geometry which has a contraction width of 2.0 mm is suitable for droplet breakup. Fabrication of the droplet generator was done with reference to the parameters obtained by the numerical simulation. Layers based fabrication method was presented, and the significant advantage of layers based fabrication was that the droplet generator can be fabricated in micro scale using micromachining techniques used in microfabrication. Fabrication method used in this study, successfully presented proper bonding without leakages, deformation or air bubbles between the sheets.

Initially, flow rates with respective to varying pumping voltages for two phases were obtained separately by experiment. Then, pumping voltage values which successfully generate droplets were identified, and respective flow rate ratios were obtained in a range of 1.04–4.74. Images were captured for different flow rate ratios within the acquired range and were processed to calculate the droplet diameter. Hereby, image based morphology identification performed satisfactorily in extracting droplet area and perimeter for calculating droplet diameter. Results show that the droplet diameter was decreased with respective decrements of flow rate ratios. Droplet diameter decreased from 3.07 mm to 1.28 mm. But, droplet generation was not observed when the flow rate ratio was decreased below value 1 using this experimental setup. The observed results for droplet diameters show a relationship with the flow rate ratios. Therefore, this relation can be utilised to control the droplet diameters by using a feedback control method.

In future, this design can be incorporated as a miniaturised system by implementing two micro-pumps, in order to further reduce the droplet diameter range. Effect of the surface roughness and the use of surfactants in surface modification will be evaluated in order to improve the uniformity of droplet formation. Furthermore, real-time image processing of the droplets can be implemented to evaluate the droplet diameter, to control the frequency of droplet generation, and can be used as a feedback control method. Neural networks, machine learning, deep learning, and artificial intelligence based methods can be utilised in image processing to introduce an autonomous approach to the droplet generation system. Ultimately, an optimised and a miniaturised design can be integrated into a LOC device as the droplet generator for biomedical applications.

Declaration of competing interest

The authors declare that they have no known competing financial interests or personal relationships that could have appeared to influence the work reported in this paper.

Acknowledgements

The authors would like to express their gratitude to the Accelerating Higher Education Expansion and Development (AHEAD) - Development Oriented Research grant (DOR-72) of the Centre for Advanced Mechatronic Systems (CFAMS), University of Moratuwa, Sri Lanka for their financial contribution and the CFAMS for their valuable advices and guidance towards the success of the research. Further, authors would like to acknowledge the facilities given by the Mechatronics Systems Laboratory at Department of Mechanical Engineering and the Latex Technology Laboratory at Department of Chemical and Process Engineering, University of Moratuwa.

References

[1] K. Douféne, C. Tourné-Péteilh, P. Etienne, A. Aubert-Pouëssel, Microfluidic systems for droplet generation in aqueous continuous phases: a focus review, Langmuir 35 (2019) 12597–12612, https://doi.org/10.1021/acs.langmuir.9b02179
[2] N., Azizipour, R., Avazpour, D.H., Rosenzweig, M., Sawan, A., Ajji, Evolution of biochip technology: a review from lab-on-a-chip to organ-on-a-chip, Micromachines 11 (6) (2020). ⟨https://doi.org/599.10.3390/mi11060599⟩; ⟨www.mdpi.com/2072-666X/11/6/599⟩.
[3] W., Asghar, M., Sher, N.S., Khan, J.M., Vyas, U., Demirci, Microfluidic chip for detection of fungal infections, ACS Omega 4 (4) (2019) 7474–7481, Publisher: American Chemical Society. ⟨https://doi.org/10.1021/acsomega.9b00499⟩.
[4] P. Sajeesh, A.K. Sen, Particle separation and sorting in microfluidic devices: a review, Microfluid. Nanofluid. 17 (2014) 1–52, https://doi.org/10.1007/s10404-013-1291-9
[5] L. Sun, F. Bian, Y. Wang, Y. Wang, X. Zhang, Y. Zhao, Bioinspired programmable wettability arrays for droplets manipulation, Proc. Natl. Acad. Sci. USA 117 (2020) 4527–4532, https://doi.org/10.1073/pnas.1921281117
[6] C. Yang, Z. Zhang, G. Li, Programmable droplet manipulation by combining a superhydrophobic magnetic film and an electromagnetic pillar array, Sens. Actuators B Chem. 262 (2018) 892–901, https://doi.org/10.1016/j.snb.2018.02.074 https://linkinghub.elsevier.com/retrieve/pii/S0925400518303526.
[7] S.-Y. Teh, R. Lin, L.-H. Hung, A.P. Lee, Droplet microfluidics, Lab Chip 8 (2) (2008) 198.10.1039/b715524g http://xlink.rsc.org/?DOI=b715524g.
[8] B. Bhushan (Ed.), Springer Handbook of Nanotechnology, Springer Handbooks, Springer, Berlin Heidelberg, Berlin, Heidelberg, 2017. ⟨https://doi.org/10.1007/978-3-662-54357-3⟩.
[9] G., Tang, J., Jin, Q., Chen, S., Di, R., Du, Simulations of centrifugal microfluidic droplet formation using two-phase level set method, in: 2014 International Conference on Manipulation, Manufacturing and Measurement on the Nanoscale (3M-NANO), IEEE, Taipei, Taiwan, 2014, 155–159. ⟨https://doi.org/10.1109/3M-NANO.2014.7057297⟩; ⟨http://ieeexplore.ieee.org/document/7057297/⟩.
[10] Z.Z., Chong, S.H., Tan, A.M., Gañán-Calvo, S.B., Tor, N.H., Loh, N.-T., Nguyen, Active droplet generation in microfluidics, Lab on a Chip 16 (1) (2016) 35–58. ⟨https://doi.org/10.1039/C5LC01012H⟩; ⟨http://xlink.rsc.org/?DOI=C5LC01012H⟩.
[11] L.L., Van, T.T., Bui, C.N., Nhu, A.N., Ngoc, T.X., Dinh, L.B., Dang, C., Tran, T.C., Duc, V. T., Dau, Simulation and experimental study of a synthetic jet valveless pump, IEEE/ASME Transactions on Mechatronics 25 (3) (2020) 1162–1170. ⟨https://doi.org/10.1109/TMECH.2019.2960332⟩.
[12] N.R. Beer, E.K. Wheeler, L. Lee-Houghton, N. Watkins, S. Nasarabadi, N. Hebert, P. Leung, D.W. Arnold, C.G. Bailey, B.W. Colston, On-chip single-copy real-time reverse-transcription PCR in isolated picoliter droplets, Anal. Chem. 80 (2008) 1854–1858, https://doi.org/10.1021/ac800048k
[13] N., Malekjani, S.M., Jafari, Simulation of food drying processes by Computational Fluid Dynamics (CFD); recent advances and approaches, Trends in Food Science & Technology, 78 (2018) 206–223. ⟨https://doi.org/10.1016/j.tifs.2018.06.006⟩; ⟨https://linkinghub.elsevier.com/retrieve/pii/S092422441730818X⟩.
[14] B.K., Gale, A.R., Jafek, C.J., Lambert, B.L., Goenner, H., Moghimifam, U.C., Nze, S.K., Kamarapu, A Review of Current Methods in Microfluidic Device Fabrication and Future Commercialization Prospects, Inventions 3 (3) (2018) 60, Number: 3 Publisher: Multidisciplinary Digital Publishing Institute. ⟨https://doi.org/10.3390/inventions3030060⟩; ⟨https://www.mdpi.com/2411-5134/3/3/60⟩.
[15] S. Prakash, S. Kumar, Fabrication of microchannels: a review, Proc. Inst. Mech. Eng. Part B J. Eng. Manuf. 229 (2015) 1273–1288, https://doi.org/10.1177/0954405414535581
[16] H. Y., Tan, W. K., Loke, N.-T., Nguyen, Integration of PDMS and PMMA for Batch Fabrication of Microfluidic Devices, in : Proceedings of the Sixth World Congress of Biomechanics (WCB 2010) 31 (2010) 4.
[17] A., Mudugamuwa, C., Jayasundara, H., Baokun, R., Amarasinghe, Development of a Robotic System with Stand-Alone Monocular Vision System for Eco-friendly Defect Detection in Oil Transportation Pipelines, in: S.G., Scholz, R.J., Howlett, R., Setchi (Eds.), Sustainable Design and Manufacturing 2020, volume 200, Springer Singapore, Singapore, 2021, pp. 107–118, series Title: Smart Innovation, Systems and Technologies. ⟨https://doi.org/10.1007/978-981-15-8131-1_10⟩.
[18] D.F., Crawford, C.A., Smith, G., Whyte, Image-based closed-loop feedback for highly mono-dispersed microdroplet production, Scientific Reports, 7 (1) (2017)

10545. ⟨https://doi.org/10.1038/s41598-017-11254-5⟩; ⟨http://www.nature.com/articles/s41598-017-11254-5⟩.
[19] P., Zhu, L., Wang, Passive and active droplet generation with microfluidics: a review, Lab on a Chip, 17 (1) (2017) 34–75. ⟨https://doi.org/10.1039/C6LC01018K⟩; ⟨http://xlink.rsc.org/?DOI=C6LC01018K⟩.
[20] W.H.P. Sampath, S.P. Hettiarachchi, N.H.R.G. Melroy, Y.W.R. Amarasinghe, Design and Development of a droplet-based microfluidics system using laser fabrication machining techniques for a lab on a chip device, in: Y.-W. Chen, S. Tanaka, R.J. Howlett, L.C. Jain (Eds.), Innovation in Medicine and Healthcare, 192 Springer Singapore, Singapore, 2020, pp. 201–210, https://doi.org/10.1007/978-981-15-5852-8_19
[21] E., Olsson, G., Kreiss, A conservative level set method for two phase flow, J. Comput.l Phys., 210 (1) (2005) 225–246. ⟨https://doi.org/10.1016/j.jcp.2005.04.007⟩.
[22] O., Sartipzadeh, S.M., Naghib, A., Seyfoori, M., Rahmanian, F.S., Fateminia, Controllable size and form of droplets in microfluidic-assisted devices: effects of channel geometry and fluid velocity on droplet size, Mater. Sci. Eng. C, 109 (2020) 110606. ⟨https://doi.org/10.1016/j.msec.2019.110606⟩.
[23] A. Bamshad, A. Nikfarjam, H. Khaleghi, A new simple and fast thermally-solvent assisted method to bond PMMA-PMMA in micro-fluidics devices, J. Micromech. Microeng. 26 (2016) 065017, https://doi.org/10.1088/0960-1317/26/6/065017
[24] F., Munas, G., Melroy, C., Abeynayake, H., Chathuranga, R., Amarasinghe, P., Kumarage, V., Dau, D., Dao, Development of PZT Actuated Valveless Micropump, Sensors 18 (5) (2018) 1302. ⟨https://doi.org/10.3390/s18051302⟩; ⟨http://www.mdpi.com/1424-8220/18/5/1302 https://doi.org/10.3390/s18051302⟩.
[25] M.R., Behrens, H.C., Fuller, E.R., Swist, J., Wu, M.M., Islam, Z., Long, W.C., Ruder, R., Steward, Open-source, 3D-printed peristaltic pumps for small volume point-of-care liquid handling, Sci. Rep., 10 (1) (2020) 1543. ⟨https://doi.org/10.1038/s41598-020-58246-6⟩; ⟨http://www.nature.com/articles/s41598-020-58246-6⟩.
[26] J.R. Lake, K.C. Heyde, W.C. Ruder, Low-cost feedback-controlled syringe pressure pumps for microfluidics applications, PLoS One 12 (2017) e0175089, https://doi.org/10.1371/journal.pone.0175089

Samith Hettiarachchi received the B.Sc. degree in mechanical engineering from the University of Moratuwa, Sri Lanka, in 2018. He is currently a Research Assistant at the Centre for Advanced Mechatronic Systems, University of Moratuwa, Sri Lanka. His research interests include microfluidics, Computational Fluid Dynamics, and Lab-on-a- Chip devices.

Gehan Melory received the B.Sc. degree in Mechanical Engineering from the University of Moratuwa, Sri Lanka, in 2017. He is currently a mater's student at the Centre for Advanced Mechatronic Systems, University of Moratuwa, Sri Lanka. His research interests include microfluidics, micropumps, Computational Fluid Dynamics, and Lab-on-a- Chip devices.

Amith Mudugamuwa received the B.Sc. degree in Mechanical Engineering from the University of Moratuwa, Sri Lanka, in 2017. He received his MPhil in mechatronic engineering from Shandong University of Science and Technology, China in 2020. He is currently a Research Assistant at the Centre for Advanced Mechatronic Systems, University of Moratuwa, Sri Lanka. His research interests include deep learning, computer vision, and fabrication of MEMS/ NEMS devices

Peshan Sampath received the B.Sc. degree in Mechanical Engineering from the University of Moratuwa, Sri Lanka. He completed his master's degree in Mechanical Engineering from the same department. He is currently serving as a Research Manager at the Centre for Advanced Mechatronic Systems, University of Moratuwa, Sri Lanka. His research interest includes sensors and actuators, automation, robotics, biomedical devices and mechatronics. He is a Member of the Institute of Electrical and Electronics Engineers (IEEE) and an Associate Member of the Institute of Engineers, Sri Lanka (IESL).

Charith Premachandra received the B.Sc. degree in mechanical engineering from the University of Moratuwa, Sri Lanka, in 2020. He is currently a Lecturer in the Department of Mechanical Engineering, University of Moratuwa, Sri Lanka. His research interests include micro/nano sensors and actuators, robotics, and mechatronics.

Prof. Ranjith Amarasinghe received the B.Sc. degree in mechanical engineering from the University of Moratuwa, Sri Lanka. He received the master's degree in information science and systems engineering and the Dr.Eng. degree in micro-electro-mechanical systems from Ritsumeikan University, Japan. He served as a Post-Doctoral Fellow under the Japan Society for the Promotion of Science and as a Chair Professor with the Department of Micro Systems Technology, Ritsumeikan University, Japan. He is currently a Professor with the Department of Mechanical Engineering, University of Moratuwa. He is also working as the Director of Centre for Advanced Mechatronic Systems (CFAMS), a multidisciplinary research centre of University of Moratuwa. His research interests include design and development of MEMS/NEMS-based devices and systems, micro/nano sensors and actuators, microrobotics, and micromechatronics.

Dr. Van Dau received the B.S. degree in aerospace engineering from Hochiminh City Udevices,ty of Technology, Vietnam, in 2002, and the M.S. and Ph.D. degrees in micromechatronics from Ritsumeikan University, Japan, in 2004 and 2007, respectively. From 2007–2009, he was a Postdoctoral Fellow with Japan Society for the Promotion of Science (JSPS) at Micro Nano Integrated Devices Laboratory, Ritsumeikan University. He is currently a Lecturer with School of Engineering and Built Environment, Griffith University, Australia. His research interests include micro-devices and microfluidics, electrohydrodynamic, nanofiber and flexible electronics, and nanoparticle, aerosol and respiratory medical device.